Journal of Biomechanics 122 (2021) 110398

Contents lists available at ScienceDirect

Journal of Biomechanics

journal homepage: www.elsevier.com/locate/jbiomech
www.JBiomech.com

Computational investigation of platelet thrombus mechanics and stability in stenotic channels

Jian Du [a], Elise Aspray [a], Aaron Fogelson [b,*]

[a] Department of Mathematical Sciences, Florida Institute of Technology, Melbourne, FL 32940, United States
[b] Departments of Mathematics and Biomedical Engineering, University of Utah, Salt Lake City, UT 84102, United States

ARTICLE INFO

Article history:
Accepted 3 March 2021

Keywords:
Arterial thrombosis
vWF-GPIbα binding
Fibrinogen-$\alpha_{IIb}\beta_3$ binding
Multiphase flow
Poroviscoelastic material

ABSTRACT

The stability of a platelet thrombus under flow is believed to depend strongly on the local hemodynamics and on the thrombus' porosity, permeability, and elasticity. A two-phase continuum model is used to investigate the biomechanics of thrombus stability in stenotic channels. It treats the thrombus as a porous, viscoelastic material moving differently than the background fluid. The dynamic clot-flow interaction is modeled through a frictional drag term. The model explicitly tracks the formation and breaking of interplatelet molecular bonds, which directly determine the viscoelastic property of the thrombus and govern its ability to resist fluid drag. We characterize the stability/fragility of thrombi for various flow speeds, porosities, bond concentrations, and bond types.

1. Introduction

The formation of an intravascular blood clot (thrombus) in a stenotic artery is dominated by the processes of platelet adhesion to the vessel wall and platelet aggregation with other platelets. Under high shear arterial conditions, the ability of a platelet aggregate to form and remain intact is determined by interactions between fluid dynamics and multiple attachment processes mediated by protein receptors on platelet surfaces and bridging proteins in the plasma. As platelets aggregate during thrombus formation, they create a porous network with voids and channels. The spatial extent and porosity of the thrombus changes with time as additional platelets are recruited to it and individual platelets or pieces of the thrombus break away.

Interactions of the plasma proteins von Willebrand factor (vWF) and fibrinogen with platelet GPIbα and $\alpha_{IIb}\beta_3$ integrin receptors, respectively, mediate platelet-platelet binding by bridging between receptors on different platelets (Fogelson and Neeves, 2015). These bond types are distinguished by whether the platelet is required to have been previously activated and by having substantially different kinetics. Fibrinogen-$\alpha_{IIb}\beta_3$ binding requires activation while vWF-GPIbα binding does not. Formation and breaking of $\alpha_{IIb}\beta_3$-mediated bonds is slow compared to that of GPIbα-mediated bonds (Arya et al., 2002; Doggett et al., 2002; Wellings and Ku, 2012; Yago et al., 2008). The breaking rates of both types of bond change with load; fibrinogen-$\alpha_{IIb}\beta_3$ are "slip" bonds (Litvinov et al., 2011) while vWF-GPIbα exhibit "catch" and "slip" behaviors depending on load (Yago et al., 2008). These differences influence the bonds' effectiveness under different flow regimes.

Intraclot advective and diffusive transport has received increased attention recently (Leiderman and Fogelson, 2011; Leiderman and Fogelson, 2013; Mirramezani et al., 2018; Tomaiuolo et al., 2014; Welsh et al., 2014) and several groups have measured thrombus permeability. Wufsus et al. (2013) measured permeability of fibrin clots and platelet-fibrin clots formed under *static* conditions over the full range of volume fractions relevant during (patho) physiological clot formation, but their relevance for thrombi formed under fast flow is unclear. Others (Muthard and Diamond, 2012; Kobayashi et al., 2017; Du et al., 2020) have measured permeability of thrombi formed under fast flow but at only one volume fraction estimated after the flow was stopped. Our recent studies (Du et al., 2020) measured the permeability of platelet-dominated thrombi formed under arterial flow conditions; we found that the permeabilities of these thrombi are 10^4-10^5-fold greater than those measured at the same volume fraction in static clots.

Platelets and arteries have very different spatial scales. Dynamic interactions at the platelet scale are critical to events at the vessel scale. Our two-phase platelet aggregation model (Du et al., 2020; Du and Fogelson, 2018) is at the vessel scale. However, it was derived from an underlying *two-scale* model in which both the vessel scale and much smaller platelet scale are treated. That model explicitly tracks the distribution of protein-mediated bonds between platelets based on the bonds' location, orientation, and

* Corresponding author.
E-mail address: fogelson@math.utah.edu (A. Fogelson).

https://doi.org/10.1016/j.jbiomech.2021.110398
0021-9290/

length, and uses the distribution function to define the stresses that the bonds exert when stretched. Because our model comes from a two-scale model, there is a relationship between parameters of the macroscale model and cell- and molecular-level measurements available in the literature. Our model is a two-phase mixture model in which the fluid and the bound platelets can move at different velocities. The use of two phases is critical because it allows thrombi with platelet number densities of 100–200-fold that of the bulk blood to form in 100-120s as observed in experiments, behaviors not captured with our earlier single-phase models (Fogelson, 1992; Fogelson and Guy, 2004; Fogelson and Guy, 2008).

Other continuum models of platelet aggregation treat the edge of the growing thrombus as a moving boundary and ignore the mechanics of the thrombus itself (Weller, 2010; Tokarev et al., 2012; Storti et al., 2014), or as an irreversibly growing impermeable elastic solid (Storti and van de Vosse, 2014), or as a single phase viscoelastic material (Anand et al., 2005). Recently, Xu et al. (2017) and Zheng et al. (2020) used phase-field models to study the mechanics of a preformed thrombus. These models handle the thrombus' mechanical properties using an energy functional without explicit reference to bond formation and breaking.

Below, we sketch our two-phase continuum model of platelet aggregation and apply it investigate the stability of preformed thrombi in arterial stenoses and their tendency to erode or embolize. In particular, we examine how the flow conditions, the solid volume fraction of the thrombus, the density of interplatelet bonds, and the type of bonds influence stability and embolization.

2. Two-phase continuum model for platelet aggregation

In this section, we describe a reduced two-phase model for mechanical interactions between background flow and preformed thrombi. See (Du and Fogelson, 2018; Du et al., 2020) for discussions of the full model.

2.1. Coupled movement of bulk blood and thrombus

The model tracks the number densities ϕ_{bu} and ϕ_{ba} of bound unactivated platelets and bound activated platelets, Eqs. (1)–(2), as these platelets move with velocity $\mathbf{u}_b$, and unbind from existing thrombi with rates f^u_{bu} and f^a_{ba}. For individual platelets that have detached from a thrombus, the number densities are ϕ_u (unactivated) and ϕ_a (activated), and these platelets advect with fluid velocity $\mathbf{u}_f$ and diffuse, Eqs. (3)–(4). Since the focus of this paper is to study the stability of existing thrombi under flow, the binding of mobile platelets is not considered.

$$(\phi_{bu})_t + \nabla\cdot(\mathbf{u}_b\phi_{bu}) = -f^u_{bu} \tag{1}$$

$$(\phi_{ba})_t + \nabla\cdot(\mathbf{u}_b\phi_{ba}) = -f^a_{ba} \tag{2}$$

$$(\phi_u)_t + \nabla\cdot(\mathbf{u}_f\phi_u) = \nabla\cdot(D\nabla\phi_u) + f^u_{bu} \tag{3}$$

$$(\phi_a)_t + \nabla\cdot(\mathbf{u}_f\phi_a) = \nabla\cdot(D\nabla\phi_a) + f^a_{ba} \tag{4}$$

The model treats the bulk blood as a viscous Newtonian fluid and the bound platelets as a viscoelastic fluid. At any spatial point, there can be a mixture of these fluids as described by their volume fractions. The fluids move according to the coupled momentum equations (5)–(6) and the incompressibility condition (7):

$$\rho_f\big((\theta_f\mathbf{u}_f)_t + \nabla\cdot(\theta_f\mathbf{u}_f\mathbf{u}_f)\big) = -\theta_f\nabla p + \nabla\cdot(\theta_f\underline{\underline{\sigma}}^{fv}) + C_3\frac{\theta_b^{\,2}}{(1-\theta_b)^3}(\mathbf{u}_b-\mathbf{u}_f). \tag{5}$$

$$\rho_b\big((\theta_b\mathbf{u}_b)_t + \nabla\cdot(\theta_b\mathbf{u}_b\mathbf{u}_b)\big) = -\theta_b\nabla p + \nabla\cdot(\theta_b\underline{\underline{\sigma}}^{bv}) + \nabla\cdot(\theta_b\underline{\underline{\sigma}}^{b}) + C_3\frac{\theta_b^{\,2}}{(1-\theta_b)^3}(\mathbf{u}_f-\mathbf{u}_b). \tag{6}$$

$$\nabla\cdot(\theta_f\mathbf{u}_f + \theta_b\mathbf{u}_b) = 0. \tag{7}$$

θ_b is the volume fraction of thrombus-bound platelets, $\theta_b = v_{plt}(\phi_{bu}+\phi_{ba})$, with v_{plt} the volume of an individual platelet. $\theta_f = 1-\theta_b$ is the fluid volume fraction; p is a Lagrange multiplier (pressure), which enforces condition (7). $\underline{\underline{\sigma}}^{fv}$ and $\underline{\underline{\sigma}}^{bv}$ are the viscous stress tensors for the two fluids, defined by:

$$\underline{\underline{\sigma}}^{fv} = \mu_f\big(\nabla\mathbf{u}_f + \nabla\mathbf{u}_f^T\big) + (\lambda_f\nabla\cdot\mathbf{u}_f)\underline{\underline{I}} \tag{8}$$

$$\underline{\underline{\sigma}}^{bv} = \mu_b\big(\nabla\mathbf{u}_b + \nabla\mathbf{u}_b^T\big) + (\lambda_b\nabla\cdot\mathbf{u}_b)\underline{\underline{I}}. \tag{9}$$

We set $\lambda_{b,f} = -\mu_{b,f}$ so that the bulk viscosities for both phases are zero. The movement of the bound platelets and the background fluid are coupled through (7) and by interphase drag forces represented by the last term in Eqs. (5)–(6). This term uses the Kozeny-Carman formula (McCabe et al., 2004) to relate drag to the platelet volume fraction θ_b. Our way of choosing the value of C_3 is discussed in Du et al. (2020). $\underline{\underline{\sigma}}^{b}$ in (6) is the viscoelastic stress tensor due to interplatelet bonds.

Since platelet activation does not play a role in the simulations reported in this paper, we do not discuss how we model it. For a description of our model of platelet activation, see (Du et al., 2020).

2.1.1. Biomechanics of interplatelet bonds

Platelet-platelet cohesion is mediated by molecular bonds that form when specific plasma proteins bind to specific receptors on the surfaces of two platelets (Fogelson and Neeves, 2015). We consider two types of bonds: (1) The protein vWF forms a bridge between GPIbα receptors on two platelets. We call this a "GG" bond for GPIbα-vWF-GPIbα. We consider GG bonds only between pairs of unactivated platelets. (2) Fibrinogen bridges between $\alpha_{IIb}\beta_3$ receptors on two activated platelets' surfaces. We call this an "AA" bond for $\alpha_{IIb}\beta_3$-fibrinogen-$\alpha_{IIb}\beta_3$.

Let $z_{GG}(\mathbf{x},t)$ and $z_{AA}(\mathbf{x},t)$ be the number densities of bonds that connect platelets at location $\mathbf{x}$ to platelets elsewhere. Let $\underline{\underline{\sigma}}^{GG}(\mathbf{x},t)$ and $\underline{\underline{\sigma}}^{AA}(\mathbf{x},t)$ denote the corresponding viscoelastic stress tensors. In this paper, the tensor $\underline{\underline{\sigma}}^{b}$ in Eq. (6) is replaced by *either* $\underline{\underline{\sigma}}^{AA}$ *or* $\underline{\underline{\sigma}}^{GG}$ depending on which type of bond is being considered. The evolution equations for the bond number density and bond stress tensor are derived in Du and Fogelson (2018) from the underlying two-scale model:

$$(z_j)_t + \nabla\cdot(\mathbf{u}_b z_j) = \alpha_j - \beta_j z_j, \tag{10}$$

$$(\underline{\underline{\sigma}}^{j})_t + \nabla\cdot(\mathbf{u}_b\underline{\underline{\sigma}}^{j}) = \underline{\underline{\sigma}}^{j}\underline{\underline{\nabla\mathbf{u}_b}} + (\underline{\underline{\sigma}}^{j}\underline{\underline{\nabla\mathbf{u}_b}})^T + C_4\alpha_j\underline{\underline{I}} - \beta_j\underline{\underline{\sigma}}^{j}, \tag{11}$$

for $j = GG, AA$. Here, α_j and β_j are the formation rate and breaking rate for bonds of type j. Using Eqs. (10)–(11), we can show that the tensor $\underline{\underline{\tau}}^{j} = \underline{\underline{\sigma}}^{j} - C_4 z_j\underline{\underline{I}}$ satisfies an Upper-convected Maxwell equation with elastic modulus $G_j = C_4 z_j$ and relaxation time $\lambda = 1/\beta_j$. (See Supplement of Du et al. (2020)).

The breaking rate of a bond depends on the force that bond is bearing (Litvinov et al., 2011; Yago et al., 2008), and we can compute the force from the bond stiffness and the bond's elongation from its rest length. From the two-scale model, we know that the local average bond length for bonds of type j is approximated by

$$<|\mathbf{y}|>_j(\mathbf{x},t) \approx \sqrt{<|\mathbf{y}|^2>_j(\mathbf{x},t)} = \sqrt{\frac{2}{S_j^0}\frac{\mathrm{Tr}(\underline{\underline{\sigma}}^{j}(\mathbf{x},t))}{z_j(\mathbf{x},t)}}, \tag{12}$$

where S_j^0 is the stiffness coefficient and "Tr" denotes the trace of the tensor (Du and Fogelson, 2018). We use $<|\mathbf{y}|>_j$ to define the bond breaking rate functions. AA bonds are slip bonds (Litvinov et al., 2011) and are assumed to obey Bell's law (Bell, 1978).

$$\beta_{AA} = \begin{cases} \beta_{AA}^0 & \text{if } <|\mathbf{y}|>_{AA} \leqslant R_{AA}, \\ \beta_{AA}^0 e^{\lambda_{AA} S_{AA}^0 (<|\mathbf{y}|>_{AA} - R_{AA})} & \text{if } <|\mathbf{y}|>_{AA} > R_{AA}. \end{cases} \tag{13}$$

GG bonds have both catch and slip characteristics (Yago et al., 2008):

$$\beta_{GG} = \begin{cases} \beta_{GG}^0 & \text{if } <|\mathbf{y}|>_{GG} \leqslant R_{GG}, \\ \beta_{GG}^0 e^{\lambda_{GG}^1 S_{GG}^0 (<|\mathbf{y}|>_{GG} - R_{GG})} & \text{if } R_{GG} << |\mathbf{y}|>_{GG} \leqslant R_c, \\ \beta_{GG}^1 e^{\lambda_{GG}^2 S_{GG}^0 (<|\mathbf{y}|>_{GG} - R_{GG})} & \text{if } <|\mathbf{y}|>_{GG} > R_c. \end{cases} \tag{14}$$

R_{AA} and R_{GG} are bond rest lengths, and R_c is the bond length at which the catch to slip bond transition happens. Fig. 1 shows the average bond lifetime $(1/\beta)$ as a function of the bond force. Table 1 gives a complete list of model parameter values.

In this paper, we choose $\alpha_{GG} = \alpha_{AA} = 0$ unless otherwise specified. Breaking of a platelet bond releases a platelet from a thrombus if that bond is the *last one* connecting that platelet to the thrombus. The rates at which bound platelets detach and become mobile are $f_{bu}^u = \beta_{GG} z_{GG} P_1$ and $f_{ba}^a = \beta_{AA} z_{AA} P_1$ for unactivated and activated bound platelets. P_1 is the probability that the bond broken is the last one for a platelet. We calculate it assuming that the numbers of GG and AA bonds/platelet are Poisson-distributed with means $\frac{z_{GG}}{\phi_{bu}}$ and $\frac{z_{AA}}{\phi_{ba}}$.

3. Results

We present results for the mechanical interactions between flowing blood and existing thrombi situated within a two-dimensional stenotic flow channel. Fig. 2 shows our two simulation setups. The flow channel is height 1×4 mm. In Fig. 2(a), the stenotic region has semi-major/minor axes of 0.413 mm and 0.333 mm. In Fig. 2(b), the two semi-ellipses have semi-major/minor axes of 0.333 mm and 0.243 mm. We prescribe the initial distribution of bound platelets to give the thrombus a core-shell structure, as observed experimentally (Van Gestel et al., 2002; Stalker et al., 2013). These regions have respective platelet volume fractions 0.30 and 0.15, corresponding to platelet number densities about 100- and 50-fold that in the bulk blood. Both $\mathbf{u}_f$ and $\mathbf{u}_b$ satisfy no-slip conditions on the vessel walls and homogeneous Neumann conditions at the inlet and outlet. The fluids are initially at rest. A constant background force in the positive x-direction is applied to accelerate the flow and the fluid velocities would reach an approximate steady-state (in the absence of embolizing thrombi) in about 0.05–0.07 s. We show simulation results up to time 0.175s. In our simulations, which do not include activation and new platelet deposition, major changes to the thrombus have occured by the time we stop the simulations.

Table 1
Values of Parameters.

Parameter	Definition	Value	Reference
ρ_f / ρ_b	Fluid and bound platelet density	1 g/cm^3	–
μ_f	Fluid viscosity	0.04 g/(cm·s)	Fogelson and Neeves (2015)
μ_b	Bound platelet viscosity	$100\mu_f$	–
v_{plt}	Platelet volume	10^{-11}cm^3	Fogelson and Neeves (2015)
ϕ_0	Blood platelet number density	3×10^8/cm^3	Fogelson and Neeves (2015)
D	Mobile platelet diffusion coefficient	10^{-7} cm^2/s	Goldsmith and Karino (1987)
C_3	Coefficient in drag formula in Eqs. (5), (6)	5×10^6 g/(cm^{3}s)	Du et al. (2020)
C_4	Coefficient in stress Eq. (11)	$\frac{5}{3} \times 10^{-10}$ g · cm^2/s^2	Du and Fogelson (2018)
R_{AA}/ R_{GG}	Rest length of bond	10^{-5} cm	Bennett (2005) and Weisel and Litvinov (2017)
S_{AA}^0/ S_{GG}^0	Stiffness of bond	10 pN/nm	Chtcheglova et al. (2004)
β_{AA}^0	Breaking rate of unstretched AA bond	0.06 s^{-1}	Litvinov et al. (2011)
λ_{AA}	Constant for strain dependent breaking rate in (13)	0.064/pN	Litvinov et al. (2011)
β_{GG}^0	Breaking rate of unstretched GG bond	9.7 s^{-1}	Yago et al. (2008)
R_c	Catch-slip transition length	102 nm	Yago et al. (2008)
β_{GG}^1	Constant for strain dependent breaking rate in (14)	1.256 s^{-1}	Yago et al. (2008)
λ_{GG}^1	Constant in (14)	−0.06/pN	Yago et al. (2008)
λ_{GG}^2	Constant in (14)	0.0422/pN	Yago et al. (2008)
K_{AA}^{bb}	AA bond formation rate	1.6×10^5/(M · s)	Yan et al., 2000
n_{AA}^{max}	Number of $\alpha_{IIb}\beta_3$ receptors on a platelet surface	50,000	Fogelson and Neeves (2015)

3.1. Thrombus stability under different flow conditions

We use the setup in Fig. 2(a) to investigate thrombus stability for three flow conditions. We assume that the thrombus contains

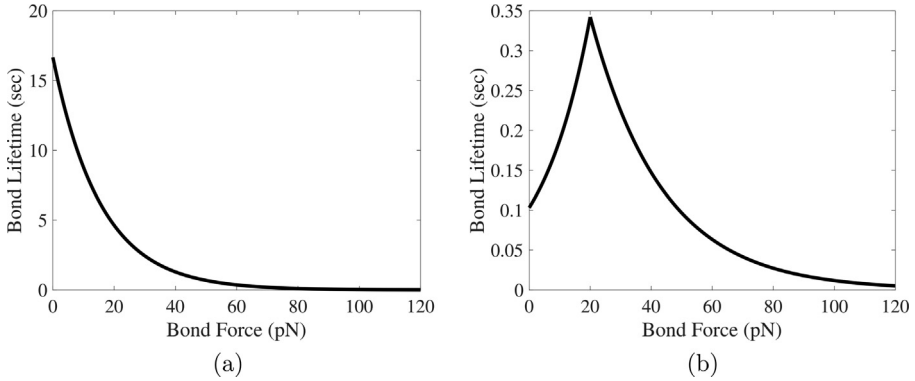

Fig. 1. Mean bond life time under force for (a) $\alpha_{IIb}\beta_3$-fibrinogen-$\alpha_{IIb}\beta_3$ (AA) bonds and (b) GPIbα-vWF-GPIbα (GG) bonds.

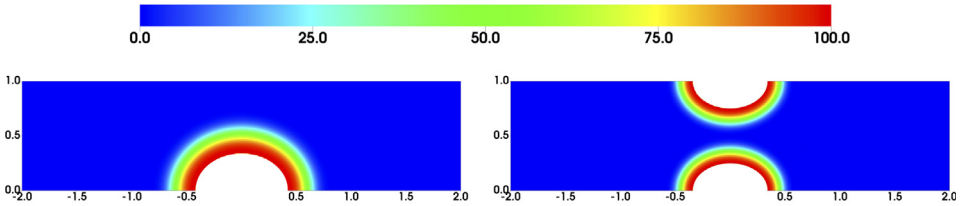

Fig. 2. Initial thrombus profiles. The number density of bound platelets (ϕ_{ba} or ϕ_{bu}), scaled by the platelet number density in the bulk blood $\phi_0 = 3 \times 10^8/\text{cm}^3$.

only activated platelets and AA bonds. We choose the initial bond density z_{AA} so that each platelet averages 5000 bonds. The initial elastic moduli ($C_4 z_{AA}$) for the thrombus core and shell are $\approx$ 2500 Pa and 1250 Pa, within the range measured experimentally (Robinson et al., 2013; Brophy et al., 2005; Schmitt et al., 2011). Fig. 3 shows ϕ_{ba} and $\mathbf{u}_f$ at $t = 0.058$ s and 0.15 s. For the lowest flow rate, Fig. 3(a,b), the thrombus is largely intact at the simulation's end. Small emboli are shed from the shell region and carried downstream. For a faster flow, large pieces break off from the thrombus (Fig. 3 (c,d)). Still greater thrombus erosion occurs at the highest flow (Fig. 3(e,f)). At $t = 0.15$ s, ≈ 0.96, ≈ 0.84 and ≈ 0.67 of the initial total number of bound platelets remain in Fig. 3(b,d,f). The denser and less permeable core is more stable under flow than is the shell. Fig. 4(a,b) show the mobile activated platelet field ϕ_a corresponding to Fig. 3(a,e). These platelets result from detachment of individual platelets from a thrombus. We see that the reduction in thrombus size at the higher shear rate results from both dislodgement of large emboli and unbinding of many individual platelets. (Video3-ab and Video3-ef in the Supplement contain animations of the simulations depicted in Fig. 3(a,b) and (e,f), respectively. Supplement Video4-a and Video4-b contain animations of the variables depicted in Fig. 4(a) and (b), respectively.)

In Fig. 5, we plot the drag force and bond breaking rate for the lowest and highest flow rates. For the highest, the drag has maximum magnitude ≈ 10 times that for the lowest. For both, the drag forces are largest near the edge of the thrombi, because of fast flow through those lower density regions. In Fig. 5(a), small drag forces cause only moderate stretching of the bonds. The thrombus' upstream edge has the highest breaking rate, $\approx$ three times that of unstretched bonds. The largest magnitude force on a bond is ≈ 20 pN, much lower than the rupture force for $\alpha_{IIb}\beta_3$-fibrinogen bonds (Litvinov et al., 2011). Thus, most of the platelet bonds remain intact. Bonds break much more rapidly for high drag (Fig. 5(b)). Along parts of the thrombus edge, the average bond lifetime $1/\beta_{AA}$ is as short as 2×10^{-3} s, leading to substantial platelet detachment.

3.2. Effect of platelet volume fraction on thrombus stability

We investigate the effect that platelet volume fraction θ_b has on mechanical stability of a thrombus. The thrombi in Fig. 6 are composed of bound activated platelets connected by AA bonds. On the left, $\theta_b \approx 0.15$ in the core and 0.075 in the shell. On the right, these values are 0.45 and 0.225, respectively. The initial bond density z_{AA} is the same as used in Section 3.1. The lower density thrombus has 10^4 bonds/platelet while the higher density one has $\approx 3.3 \times 10^3$. The same body force is applied to drive the flow.

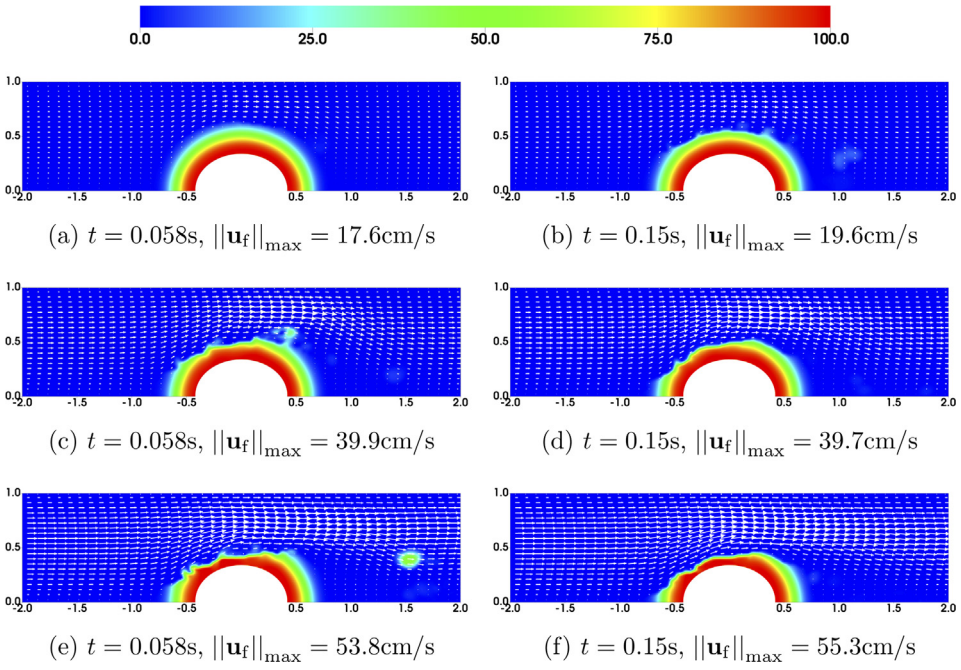

Fig. 3. Effect of flow rate on clot stability. Snapshots of the number density ϕ_{ba} of bound activated platelets and fluid velocity $\mathbf{u}_f$ driven by low (a, b), medium (c, d), and high (e, f) background force. All vectors have the same scale. Bound platelet volume fraction $\theta_b = 0.003\phi_{ba}$. Panels (d, f) show approximate steady states for their respective simulations.

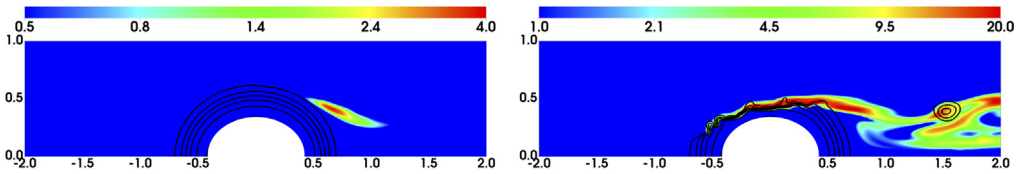

Fig. 4. Number density ϕ_a of mobile activated platelets at $t = 0.058$s (a) for the simulation in Fig. 3 for the simulation in Fig. 3(e,f). The black contour lines show the number density ϕ_{ba}. Bound platelet volume fraction $\theta_b = 0.003\phi_{ba}$. The indicated shear rate values are measured on the wall directly opposite the apex of the stenosis.

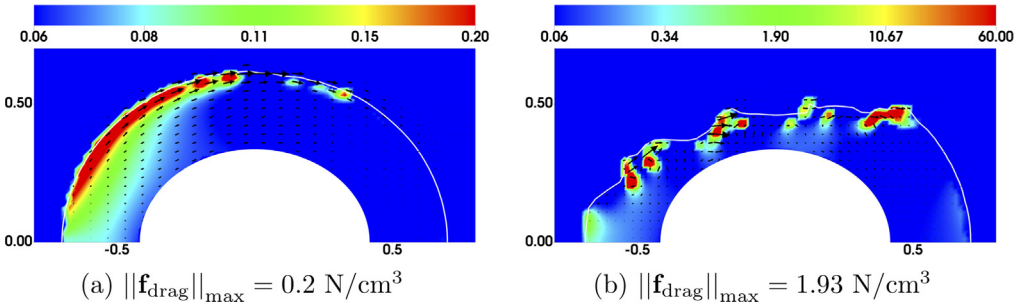

Fig. 5. The fluid drag force density and the bond breaking rate β_{AA} at $t = 0.058$s for simulation results (a) shown in Fig. 3 shown in Fig. 3(e). The vectors are scaled differently in (a) and (b). The white contour lines show $\phi_{ba} = 10$.

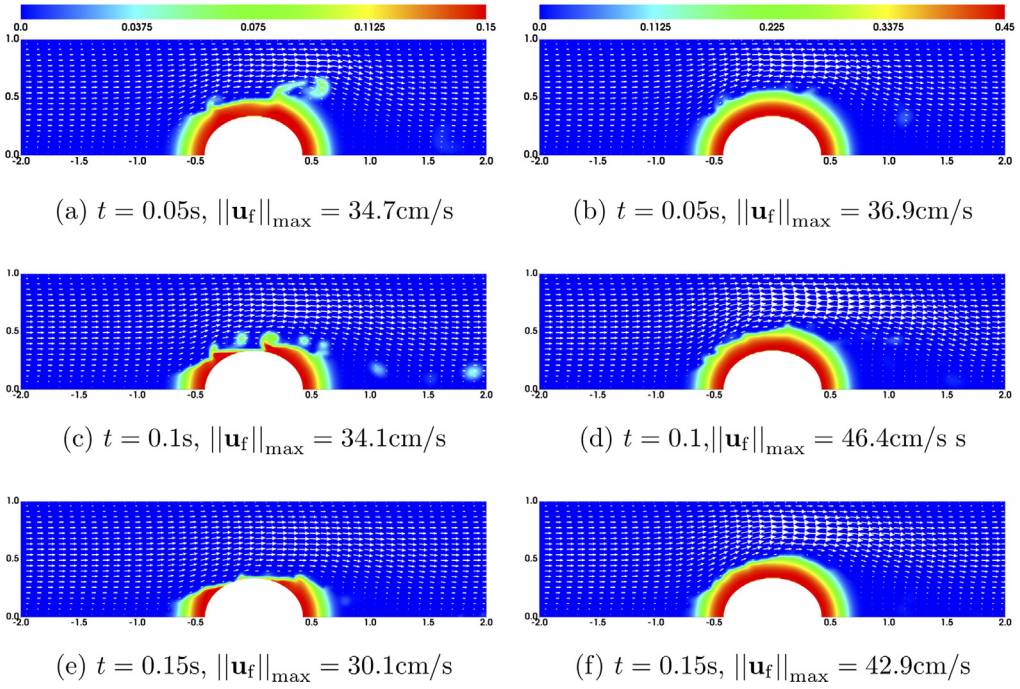

Fig. 6. Effect of initial platelet volume fraction on clot stability. The fluid velocity field $\mathbf{u}_f$ and the bound platelet volume fraction θ_b for thrombi with initial volume fractions (left) 0.15 core and 0.075 shell and (right) 0.45 shell and 0.225 shell. All vectors have the same scale. Panels (e,f) show approximate steady states for their respective simulations.

Fig. 6(a,c,e) show that the lower density thrombus undergoes repeated embolization, especially near its apex. By $t = 0.15$ s, much of the thrombus in the stenosis center has been washed away and less than half of the original platelets remain. The higher density thrombus experiences only moderate embolization at the upstream shell edge (Fig. 6) ≈ 0.87 of it remains at $t = 0.15$ s. With portions of the thrombi removed, the speed of the fluid above the stenosis decreases during the latter part of both simulations. Fig. 7 shows a zoomed look at $\|\mathbf{u}_b\|$ and the drag force density in the thrombi at $t = 0.05$ s. In Fig. 7(a), $\|\mathbf{u}_b\|$ is high in large parts of the more porous thrombus and these portions deform significantly. Platelets in the less porous thrombus (Fig. 7(b)) move much less; the motion here is predominantly along parts of the thrombus edge. A major distinction between these simulations is that large drag forces occur throughout much of the less dense thrombus, but are concentrated near the top edge for the denser thrombus

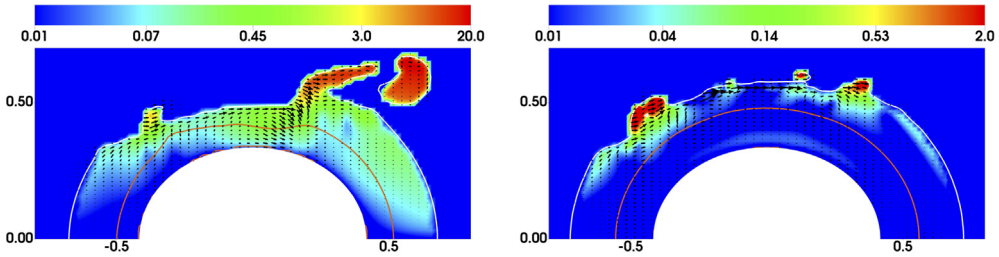

(a) $||\mathbf{f}_{\text{drag}}||_{\max} = 0.73$ N/cm^3 (b) $||\mathbf{f}_{\text{drag}}||_{\max} = 1.1$ N/cm^3

Fig. 7. The magnitude of the bound platelet velocity $||\mathbf{u}_b||$ in cm/s (color plot) and the fluid drag force density at $t = 0.05$ s, for simulations with initial volume fractions (a) 0.15 core and 0.075 shell and (b) 0.45 core and 0.225 shell. All vectors have the same scale. The black and orange contour lines are for $\phi_{ba} = 8$ and 45, respectively, in (a) and for $\phi_{ba} = 8$ and 110, respectively, in (b).

with much lower drag forces deeper inside it, consistent with the observation that the denser thrombus' core is largely intact at the simulation's end. The more porous thrombus also has more fluid penetration into its core area, especially in the region from which large emboli are peeling off. Following the removal of its outer layer, fluid penetrates deep into the thrombus' interior causing significant embolization there. (Also see Supplementary videos Video6-ace and Video6-bdf.)

3.3. Effect of interplatelet bond density on thrombus stability

We next discuss simulations with different initial bond densities. The thrombi contain only activated platelets bound by AA bonds. The rows of Fig. 8 show results with the initial number of bonds/platelet 100, 500 and 5000, and initial elastic moduli 50 Pa, 250 Pa, and 2500 Pa for the cores and half of that for the shells. The same background force is applied to drive the flow for all simulations. When starting with 100 bonds/platelet (Fig. 8(a, b)), large emboli are dislodged and swept downstream leaving small portions of the thrombus only at the up- and down-stream corners of the stenosis. With 500 bonds/platelet to start, the thrombi are more resistant to the flow (Fig. 8(c,d)). By $t = 0.05$ s, significant embolization has occurred in the thrombus shell but the core is largely intact. By $t = 0.1$ s, most of the thrombus in the stenosis neck has been carried away, with large parts of the thrombus remaining on the upstream and downstream faces of the stenosis. Fig. 8(e,f) show that with 5000 bonds/platelet, moderate erosion occurs only in the outer parts of the shell above the stenosis' apex. Most of the thrombus is essentially stationary during the entire simulation. For the simulations in Fig. 8(d,f), $\mathbf{u}_b$ and the number of bonds/platelet are plotted in Fig. 9 (see also Supplement Video9-a and Video9-b). $||\mathbf{u}_b|| \approx 0.01$ cm/s in the"red" regions of both thrombi where the number of bonds/platelet is relatively high. The maximum of $||\mathbf{u}_b||$ is ≈ 0.1 cm/s in the high bond density case with the relatively fast flow confined to a small region along the thrombus edge. With lower bond density, the movement of the platelets is faster and more widespread.

For all simulations presented above, bond breaking but not new bond formation was allowed. Here, we look at how things change when we allow formation of new bonds between *already bound*

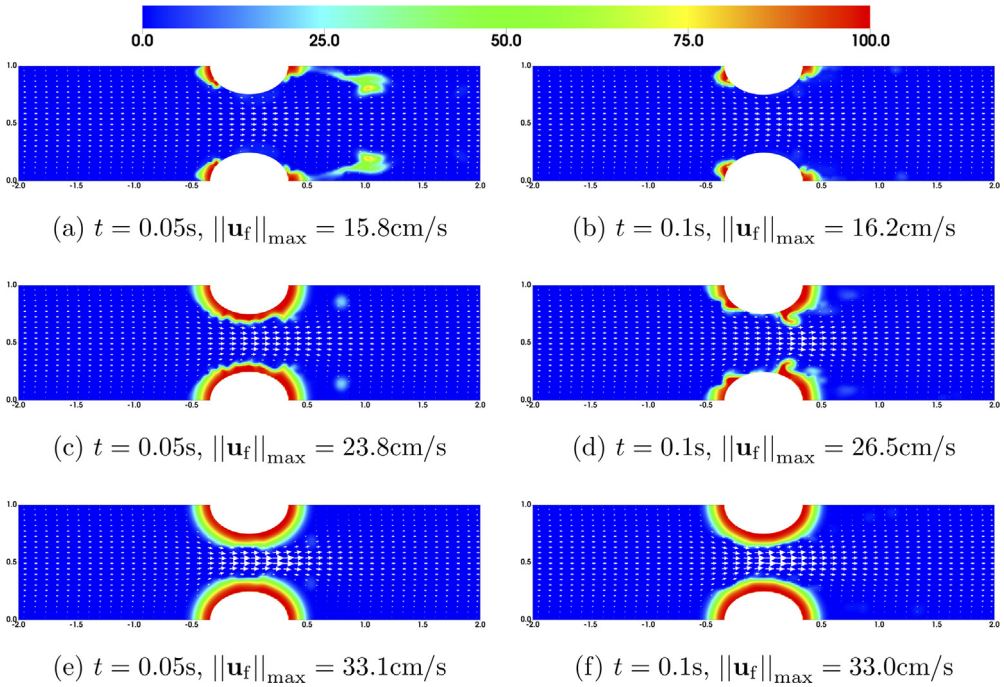

(a) $t = 0.05$s, $||\mathbf{u}_f||_{\max} = 15.8$cm/s (b) $t = 0.1$s, $||\mathbf{u}_f||_{\max} = 16.2$cm/s

(c) $t = 0.05$s, $||\mathbf{u}_f||_{\max} = 23.8$cm/s (d) $t = 0.1$s, $||\mathbf{u}_f||_{\max} = 26.5$cm/s

(e) $t = 0.05$s, $||\mathbf{u}_f||_{\max} = 33.1$cm/s (f) $t = 0.1$s, $||\mathbf{u}_f||_{\max} = 33.0$cm/s

Fig. 8. Effect of initial bond density on clot stability. The fluid velocity $\mathbf{u}_f$ and the number density ϕ_{ba} of bound activated platelets. Bound platelet volume fraction $\theta_b = 0.003\phi_{ba}$. All vectors have the same scale. The initial average number of bonds per platelet are (a,b) 100 (c,d) 500, and (e,f) 5000. Panels (f) shows an approximate steady state for the corresponding simulation.

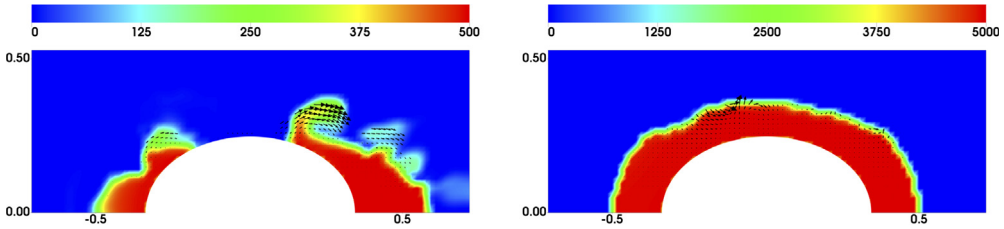

(a) $||\mathbf{u}_b||_{\max} = 4.1\text{cm/s}$ (b) $||\mathbf{u}_b||_{\max} = 0.1\text{cm/s}$

Fig. 9. Average number of bonds/platelet (color plot) and bound platelet velocity $\mathbf{u}_b$ at $t = 0.10$s for simulations with (a) 500 bonds/platelet and (b) 5000 bonds/platelet initially (corresponding to Fig. 8(d) and (f), respectively). The vectors in (a) and (b) are scaled differently.

platelets. We again consider the situation in Fig. 8(c,d), but now allow new AA bonds to form between bound platelets at rate

$$\alpha_{AA} = K_{AA}^{bb}\left(n_{AA}^{max}\phi_{ba} - 2z_{AA}\right)^2. \tag{15}$$

K_{AA}^{bb} is the second order rate constant, n_{AA}^{max} the number of $\alpha_{IIb}\beta_3$ receptors on a platelet's surface, and $n_{AA}^{max} - 2z_{AA}$ the concentration of available receptors on the platelets. All other model conditions are the same as for Fig. 8(c-d). Comparing Figs. 10(a) in the Supplement and 8(d), we see that embolization continues, but new bond formation stabilizes the thrombus and reduces erosion. Fig. 10(b) in the Supplement shows that the number of bonds/platelet grows from 500 at $t = 0$ to approximately 4000 in the core and 2000–3000 in the remaining shell. (See Supplemental videos Video8-ab and Video8-ef)

3.4. Effect of bond type on thrombus stability

Finally, we investigate how different types of bonds affect thrombus stability. AA and GG bonds differ in their formation rates and in their breaking rates' magnitudes and dependence on applied force (Table 1 and Eqs. 14). On the left of Fig. 11 in the Supplement, the thrombus contains only *bound unactivated* platelets connected by GG bonds. On the right, the thrombus is composed of bound activated platelets connected by AA bonds. All other model parameters are identical for the two simulations. We see that GG bonds by themselves do not support a stationary thrombus under fast flow. Large emboli break away, leaving only $\approx 40\%$ of the original thrombus by $t = 0.175$ s. The thrombus supported by AA bonds is much stronger under fast flow, and it exhibits moderate embolization only near its upstream edge. See Video11-ace and Video11-bdf in the Supplement.

We plot the breaking rates β_{GG} and β_{AA} in Fig. 12 in the Supplement. They are large where much embolization and deformation was seen in Fig. 11 (in the Supplement). The maximum of β_{GG} is two orders of magnitude greater than that of β_{AA}. As Fig. 13 in the Supplement shows, the number of AA bonds/platelet at $t = 0.1$ s is close to its initial value of 5000 throughout the thrombus because the AA bond's breaking rate remains low even under the forces in the simulation. By contrast, the number of GG bonds/-platelet in Fig. 13(a) in the Supplement is much lower than 5000 over the whole thrombus. (Also see Supplement Video13-a and Video13-b.) The rapid rupture of platelet GG bonds sharply reduces the thrombus's elastic modulus ($C_4 z_{GG}$), leading to substantial embolization. The remaining GG bonds are distributed unevenly. Near the upstream corner of the thrombus, the bonds/platelet value is much higher than at the downstream corner, even though shear stresses are relatively low at the downstream location. The low shear stresses at the downstream location lead to very little elongation of the bonds there and so their breaking rate is close to β_{GG}^0 (Eq. (14)). At the upstream corner of the stenosis, the shear stresses are relatively high. Most of the GG bonds there are stretched enough that they are in the catch-bond range (Fig. 1 (b)) and the bond lifetime actually increases with the applied force in this region. We note that in simulations (not shown) with non-activated platelets in the shell and activated platelets in the core at the intermediate flow rate, we saw the shell embolize and the core remain largely intact.

4. Discussion

We described our two-phase model of platelet aggregation and applied it to investigate the stability of pre-formed thrombi in stenotic arteries under a range of arterial flow conditions and assumptions about the structure and properties of the thrombus. The model consists of a unified set of equations that apply throughout the domain and which describe two-phase fluid dynamics, transport and reactions of platelet populations, and formation and breaking of interplatelet bonds. The thrombus is treated as a porous, viscoelastic material whose spatial extent and mechanical properties evolve with the development or dissolution of the thrombus; the permeability and elastic modulus at each point of the thrombus are functions of the bound platelet volume fraction and the interplatelet bond concentration at that location. The overall flow through the thrombus depends on how platelets and bonds are distributed within it. All of the model variables have readily understood physical or biological meaning (e.g., cell density, bond density, bond length) unlike some other types of models (e.g., phase-field models). Because our macroscale model is derived from an underlying two-scale model that treats processes at both the vessel and platelet scales, there is a clear interpretation of macroscale parameters in terms of microscale ones. Since those parameters pertain to the actual biological processes of bond formation and cellular aggregation, the macroscale model is informed by the numerous laboratory measurements made at the platelet or molecular scale. For example, using molecular level bond kinetic information, thrombus elastic moduli that emerge from our simulations are within the range of those estimated experimentally (Robinson et al., 2013; Brophy et al., 2005; Schmitt et al., 2011).

In Du et al. (2020) we applied the model to look at growth of a thrombus in a straight tube under arterial flow conditions. Here, we look at the stability of pre-formed thrombi in a stenotic artery under high shear conditions. These computational experiments are similar to those in Xu et al. (2017) and Zheng et al. (2020) where phase-field models were used. Each simulation involved one or two thrombi with prescribed concentric core and shell regions in the stenosis. We varied the volume fractions of bound platelets in these two regions, the concentration of interplatelet bonds, and the type of bonds (GPIbα-vWF bonds and $\alpha_{IIb}\beta_3$-fibrinogen bonds) we considered, as well as the speed of fluid entering the inlet of the domain.

We characterized the extent of embolization of large fragments and individual platelets, and related these quantities to drag forces

in the thrombi, the degree of stretch of interplatelet bonds in different regions of the thrombus, and the kinetic properties, in particular the bond breaking rate functions of different bond types. Our salient observations include:

- For a given composition and size thrombus, embolization extent and speed increases with the background flow's shear rate.
- At high shear rates, both sizable emboli and many individual platelets detach from the thrombi.
- With equal concentrations of interplatelet bonds, less dense portions of the thrombi are more fragile, and that this can be traced to the extent of fluid permeation of the thrombus.
- New bond formation can stabilize the thrombus without the binding of additional platelets.
- The kinetics of the bonds strongly influence their ability to sustain drag forces, so that multiple types of bond may be necessary for the formation and stability of thrombi under high shear, consistent with experimental evidence (Matsui et al., 2002; Ruggeri et al., 1999).
- For bonds with catch-slip breaking kinetics, more residual thrombus may be left in high shear regions than in lower shear regions.

Declaration of Competing Interest

The authors declare that they have no known competing financial interests or personal relationships that could have appeared to influence the work reported in this paper.

Acknowledgements

This work was supported, in part, by NSF grants DMS-1715156 to J.D. and DMS-1716898 to A.L.F.

Appendix A. Supplementary material

Supplementary data associated with this article can be found, in the online version, at https://doi.org/10.1016/j.jbiomech.2021.110398.

References

Anand, M., Rajagopal, K., Rajagopal, K., 2005. A model for the formation and lysis of blood clots. Pathophysiol. Haemost. Thromb. 34, 109–120.
Arya, M., Lopez, J.A., Romo, G.M., Dong, J.F., McIntire, L.V., et al., 2002. Measurement of the binding forces between von willebrand factor and variants of platelet glycoprotein ibα using optical tweezers. Lasers Surg. Med. 30, 306–312.
Bell, G., 1978. Models for the specific adhesion of cells to cells. Science 200, 618–627.
Bennett, J.S., 2005. Structure and function of the platelet integrin $\alpha_{IIb}\beta_3$. J. Clin. Invest. 115, 3363–3369.
Brophy, D.F., Martin, R.J., Gehr, T.W., Carr, M.E., 2005. A hypothesis-generating study to evaluate platelet activity in diabetics with chronic kidney disease. Thrombosis J. 3. https://doi.org/10.1186/1477-9560-3-3.
Chtcheglova, L.A., Shubeita, G., Sekatskii, S., Dietler, G., 2004. Force spectroscopy with a small dithering of afm tip: a method of direct and continuous measurement of the spring constant of single molecules and molecular complexes. Biophys. J. 86, 1177–1184.
Doggett, T.A., Girdhar, G., Lawshe, A., Schmidtke, D.W., Laurenzi, I.J., Diamond, S.L., Diacovo, T.G., 2002. Selectin-like kinetics and biomechanics promote rapid platelet adhesion in flow: The GPIbα -vWF tether bond. Biophys. J. 83, 184–205.
Du, J., Fogelson, A.L., 2018. A two-phase mixture model of platelet aggregation. Math. Med. Biol. 35, 225–256.
Du, J., Kim, D., Alhawael, G., Ku, D.N., Fogelson, A.L., 2020. Clot permeability, agonist transport, and platelet binding kinetics in arterial thrombosis. Biophys. J. 119, 2102–2115.
Fogelson, A.L., 1992. Continuum models of platelet aggregation: Formulation and mechanical properties. SIAM JAM 52, 1089–1110.
Fogelson, A.L., Guy, R.D., 2004. Platelet-wall interactions in continuum models of platelet aggregation: Formulation and numerical solution. Math. Med. Biol. 21, 293–334.
Fogelson, A.L., Guy, R.D., 2008. Immersed-boundary-type models of intravascular platelet aggregation. Comput. Meth. Appld. Mech. Eng. 197, 2087–2104.
Fogelson, A.L., Neeves, K.B., 2015. Fluid mechanics of blood clot formation. Annu. Rev. Fluid Mech. 47, 377–403.
Goldsmith, H.L., Karino, T., 1987. Interactions of human blood cells with the vascular endothelium. Ann. NY Acad. Sci. 516, 468–483.
Kobayashi, S., Komatsu, M., Ku, D.N., 2017. Convection through platelet thrombi. In: 63rd Annual SSC Meeting of the ISTH. Berlin, Germany. July 813, 2017.
Leiderman, K., Fogelson, A.L., 2011. Grow with the flow: a spatial-temporal model of platelet deposition and blood coagulation under flow. Math. Med. Biol. 28, 47–84.
Leiderman, K., Fogelson, A.L., 2013. The influence of hindered transport on the development of platelet thrombi under flow. Bull. Math. Biol. 75, 1255–1283.
Litvinov, R.I., Barsegov, V., Schissler, A.J., Fisher, A.R., Bennet, J.S., Weisel, J.W., Shuman, H., 2011. Dissociation of bimolecular $\alpha_{IIb}\beta_3$-fibrinogen complex under a constant tensile force. Biophys. J. 100, 165–173.
Matsui, H., Sugimoto, M., Mizuno, T., Tsuji, S., Miyata, S., Matsuda, M., Yoshioka, A., 2002. Distinct and concerted functions of von Willebrand factor and fibrinogen in mural thrombus growth under high shear flow. Blood 100, 3604–3610.
McCabe, W., Smith, J., Harriott, P., 2004. Unit Operations of Chemical Engineering. McGraw Hill, Englewood Cliffs, NJ. seventh ed..
Mirramezani, M., Herbig, B., Stalker, T., Nettey, L., Cooper, M., Weisel, J., Diamond, S., Sinno, T., Brass, L., Shadden, S., Tomaiuolo, M., 2018. Platelet packing density is an independent regulator of the hemostatic response to injury. J. Thromb. Haemost. 16 (5), 973–983.
Muthard, R.W., Diamond, S.L., 2012. Blood clots are rapidly assembled hemodynamic sensors: flow arrest triggers intraluminal thrombus contraction. Arteriosclerosis, Thrombosis Vasc. Biol. 32 (12), 2938–2945.
Robinson, R.A., Herbertson, L.H., Sarkar Das, S., Malinauskas, R.A., Pritchard, W.F., Grossman, L.W., 2013. Limitations of using synthetic blood clots for measuring in vitro clot capture efficiency of inferior vena cava filters. Med. Devices: Evidence Res. 6, 49–57.
Ruggeri, Z.M., Dent, J.A., Saldv ar, E., 1999. Contribution of distinct adhesive interactions to platelet aggregation in flowing blood. Blood 94, 172–178.
Schmitt, C., Henni, A.H., Cloutier, G., 2011. Characterization of blood clot viscoelasticity by dynamic ultrasound elastography and modeling of the rheological behavior. J. Biomech. 44 (4), 622–629.
Stalker, T., EA, E.T., Wu, J., Wannemacher, K.M., Cermignano, S.L., Voronov, R., Diamond, S.L., Brass, L.F., 2013. Hierarchical organization in the hemostatic response and its relationship to the platelet-signaling network. Blood 121, 1875–1885.
Storti, F., van de Vosse, F., 2014. A continuum model for platelet plug formation, growth, and deformation. Int. J. Numer. Methods Biomed. Eng. 30, 1541–1557.
Storti, F., van Kempen, T., van de Vosse, F., 2014. A continuum model for platelet plug formation and growth, International Journal for Numerical Methods in Biomedical. Engineering 30, 634–658.
Tokarev, A., Sirakov, I., Panasenko, G., Volpert, V., Shnol, E., Butylin, A., Ataullakhanov, F., 2012. A continuous mathematical model of platelet thrombus formation in blood flow. Russian J. Numer. Anal. Math. Model. 27, 191–212.
Tomaiuolo, M., Stalker, T.J., Welsh, J.D., Diamond, S.L., Sinno, T., Brass, L.F., 2014. A systems approach to hemostasis: 2. Computational analysis of molecular transport in the thrombus microenvironment. Blood 124 (11), 1816–1823.
Van Gestel, M.A., Heemskerk, J.W.H., Slaaf, D.W., Heijnen, V.V.T., Sage, S.O., Reneman, R.S., Oude Egbrink, M.G.A., 2002. Real-time detection of activation patterns in individual platelets during thromboembolism in vivo: Differences between thrombus growth and embolus formation. J. Vasc. Res. 39, 534–543.
Weisel, J.W., Litvinov, R.I., 2017. Fibrin formation, structure and properties. Subcell Biochem. 82, 405–456.
Weller, F., 2010. A free boundary problem modeling thrombus growth. J. Math. Biol. 61.
Wellings, P.J., Ku, D.N., 2012. Mechanisms of platelet capture under very high shear. Cardiovasc. Eng. Technol. 3 (2), 161–170.
Welsh, J.D., Stalker, T.J., Voronov, R., Muthard, R.W., Tomaiuolo, M., Diamond, S.L., Brass, L.F., 2014. A systems approach to hemostasis: 1. The interdependence of thrombus architecture and agonist movements in the gaps between platelets. Blood 124, 1808–1815.
Wufsus, A., Macera, N., Neeves, K., 2013. The hydraulic permeability of blood clots as a function of fibrin and platelet density. Biophys. J. 104, 1812–1823.
Xu, S., Xu, Z., Kim, O.V., Litvinov, R.I., Weisel, J.W., Alber, M., 2017. Model predictions of deformation, embolization and permeability of partially obstructive blood clots under variable shear flow. J. R. Soc. Interface 14, 20170441.
Yago, T., Lou, J., Wu, T., Yang, J., Miner, J., Coburn, L., Lopez, J., Cruz, M., Dong, J., McIntire, L., McEver, R., Zhu, C., 2008. Platelet glycoprotein ibα forms catch bonds with human wt vwf but not with type 2b von willebrand disease vwf. J. Clin. Investig. 118, 3195207.
Yan, B., Hu, D.D., Knowles, S.K., Smith, J.W., 2000. Probing chemical and conformational differences in the resting and active conformers of platelet integrin $\alpha_{IIb}\beta_3$. J. Biol. Chem. 275, 7249–7260.
Zheng, X., Yasdani, A., Li, H., Humphrey, J., Karniadakis, G.E., 2020. A three-dimensional phase-field model for multiscale modeling of thrombus biomechanics in blood vessels. PLOS Comput. Biol. 16, e1007709.